Heliyon 9 (2023) e22138

Contents lists available at ScienceDirect

Heliyon

journal homepage: www.cell.com/heliyon

Development of an EBOV MiniG plus system as an advanced tool for anti-Ebola virus drug screening

Chi-Ju Hsu [a,b,1], Cheng-Hsiu Chen [a,b,1], Wen-Ting Chen [a], Ping-Cheng Liu [a,d], Tein-Yao Chang [a,e], Meng-He Lin [a], Cheng-Cheung Chen [a,b], Hsing-Yu Chen [f], Chih-Heng Huang [a,b], Yun-Hsiang Cheng [a,c,**], Jun-Ren Sun [a,b,c,g,*]

[a] *Institute of Preventive Medicine, National Defense Medical Center, Taipei, Taiwan*
[b] *Graduate Institute of Medical Science, National Defense Medical Center, Taipei, Taiwan*
[c] *Department of Physiology and Biophysics, Graduate Institute of Physiology, National Defense Medical Center, Taiwan*
[d] *Graduate Institute of Applied Science and Technology, National Taiwan University of Science and Technology, Taiwan*
[e] *Department of Pathology and Graduate Institute of Pathology and Parasitology, Tri-Service General Hospital, National Defense Medical Center, Taiwan*
[f] *Department of Medical Techniques, Taipei City Hospital Ren-Ai Branch, Taiwan*
[g] *Division of Infectious Diseases and Tropical Medicine, Department of Internal Medicine, Tri-Service General Hospital, National Defense Medical Center, Taiwan*

ARTICLE INFO

Keywords:
minigenome
Ebola virus
Nucleocapsid protein
Human coronaviruses

ABSTRACT

The incidence of zoonotic diseases, such as coronavirus disease 2019 and Ebola virus disease, is increasing worldwide. However, drug and vaccine development for zoonotic diseases has been hampered because the experiments involving live viruses are limited to high-containment laboratories. The Ebola virus minigenome system enables researchers to study the Ebola virus under BSL-2 conditions. Here, we found that the addition of the nucleocapsid protein of human coronaviruses, such as severe acute respiratory syndrome coronavirus 2, can increase the ratio of green fluorescent protein-positive cells by 1.5–2 folds in the Ebola virus minigenome system. Further analysis showed that the nucleocapsid protein acts as an activator of the Ebola virus minigenome system. Here, we developed an EBOV MiniG Plus system based on the Ebola virus minigenome system by adding the SARS-CoV-2 nucleocapsid protein. By evaluating the antiviral effect of remdesivir and rupintrivir, we demonstrated that compared to that of the traditional Ebola virus minigenome system, significant concentration-dependent activity was observed in the EBOV MiniG Plus system. Taken together, these results demonstrate the utility of adding nucleocapsid protein to the Ebola virus minigenome system to create a powerful platform for screening antiviral drugs against the Ebola virus.

Abbreviations: The Ebola virus, (EBOV); minigenome, (MiniG); nucleocapsid protein, (N); severe acute respiratory syndrome coronavirus 2, (SARS-CoV-2); green fluorescent protein, (GFP); ribonucleoprotein, (RNP); viral RNA, (vRNA); complementary RNA, (cRNA); messenger RNA, (mRNA); glyceraldehyde-3-phosphate dehydrogenase, (GAPDH).

* Corresponding author.Institute of Preventive Medicine, National Defense Medical Center, Taipei, Taiwan.
** Corresponding author. Institute of Preventive Medicine, National Defense Medical Center, Taipei, Taiwan,
E-mail addresses: clcc0128@mail.ndmctsgh.edu.tw (Y.-H. Cheng), tsghsun@gmail.com (J.-R. Sun).
[1] These authors contributed equally to this work.

https://doi.org/10.1016/j.heliyon.2023.e22138
Received 3 August 2023; Received in revised form 21 October 2023; Accepted 5 November 2023
Available online 11 November 2023

1. Introduction

The coronavirus disease 2019 (COVID-19), which is caused by severe acute respiratory syndrome coronavirus 2 (SARS-CoV-2), has been classified as a zoonotic disease, having been acquired from animals [1–4]. In addition to SARS-CoV-2, zoonotic viruses pose a huge threat to public health worldwide. These zoonotic pathogens cause severe morbidity and mortality [1,5]; therefore, they must be handled in high-containment laboratories at biosafety levels 3 or 4 (BSL-3/4) [6–8]. Conducting research in high-containment laboratories requires many considerations, including specialized facilities and equipment, enhanced biosafety practices, and highly trained personnel [6]. However, these considerations have limited the speed of research, which includes supporting tests, laboratory diagnostic analyses, vaccine studies, and thus the development of related applications.

The Ebola virus (EBOV), a member of the genus *Ebolavirus* and the *Filoviridae* family, causes a severe disease known as viral hemorrhagic fever in humans and may harm public health worldwide [9]. Once the EBOV virus enters host cells, it releases viral genomic negative-sense (−) RNAs, which in turn transcribe viral mRNAs responsible for generating filoviral proteins. Subsequently, these RNAs undergo a shift, leading to the production of positive-sense (+) RNAs, essential for creating new viral genomic (−) RNAs. The entire process is governed by the viral ribonucleoprotein (RNP) complex, which consists of RNA-dependent RNA polymerase L, VP35 (polymerase cofactor), nucleoprotein (NP), and VP30 (transcription factor). These components represent the minimum essential elements for EBOV transcription and replication. The EBOV minigenome (EBOV MiniG) system is a reporter-based RNP activity assay which was created more than 20 years ago, has become a benchmark in this field and used to screen new antiviral drugs outside high-containment laboratories [10–14]. The EBOV MiniG system contains one minigenome plasmid and four helper plasmids (Fig. 1) [12,15]. The minigenome plasmid is a shortened version of viral templates in which all the viral genes have been removed and replaced with reporter genes, such as green fluorescent protein (GFP) or luciferase. The four helper plasmids contain proteins necessary for transcription and replication, such as the NP, VP30, VP35, and the RNA-dependent RNA polymerase L. After the cells are transfected with these five plasmids, the minigenome plasmids continuously express antisense reporter RNA as viral RNA (vRNA). The NP and the VP35, VP30, and L proteins are expressed and bind to viral vRNA to form a RNP complex. Through RNP complex interactions, vRNA is synthesized as complementary RNA (cRNA) and messenger RNA (mRNA), resulting in the production of reporter proteins [14,16].

SARS-CoV-2 belongs to the family *Coronaviridae*, which is composed of seven human coronaviruses (HCoVs) [3,4,17,18]. A total of seven HCoVs have been identified: two alpha-coronaviruses (HCoV-229E and HCoV-NL63) and five beta-coronaviruses [HCoV-HKU1, HCoV-OC43, Middle East respiratory syndrome coronavirus (MERS), SARS-CoV-1, and SARS-CoV-2]. The coronavirus genome consists of a positive-sense RNA genome of 29–30 kb, which encodes four major structural proteins: the spike (S), envelope (E), nucleocapsid (N), and membrane (M) proteins [3]. The coronavirus nucleocapsid protein has the following functions: it is assembled into viral RNA-protein complexes with a characteristic barrel shape to package viral RNA and interact with the membrane proteins to recruit the viral genome for envelopment [3,17,19,20]. Although the Ebola virus belongs to a different family from that of coronaviruses, we found that four coronavirus Ns affect the activity of the EBOV MiniG system. Therefore, we developed the EBOV MiniG Plus system by combining the EBOV MiniG system with the SARS-CoV-2 N.

2. Materials and methods

2.1. Cell culture

Human embryonic kidney (HEK293T) cells (ATCC CRL-3216, Manassas, VA, USA) were cultured in high-glucose Dulbecco's

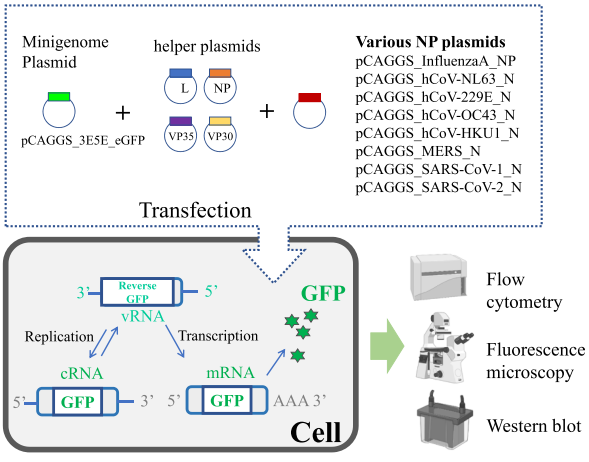

Fig. 1. Illustration of the EBOV MiniG system used here. The HEK293T cells were transfected with a combination of the minigenome plasmid and four helper plasmids with/without various plasmids expressing the nucleocapsid protein (N). At 24 and 48 h post-transfection, the green fluorescent protein (GFP) was detected using flow cytometry, fluorescence microscopy, and Western blot.

modified Eagle's medium (DMEM) (Thermo Fisher Scientific, Waltham, MA, USA) supplemented with 10 % fetal bovine serum (Avantor, Radnor, PA, USA), penicillin-streptomycin, and sodium bicarbonate (Hyclone, logan, UT, USA). Cells were grown in an incubator at 37 °C in a humid environment.

2.2. DNA plasmids and cloning

The five plasmids comprising the EBOV minigenome (EBOV MiniG) system were gifts from Elke Mühlberger (Addgene plasmid # 103049, 103050, 103051, 103052 and 103054, Watertown, MA, USA) [15]. The sequences of N of the human coronavirus

Table 1
Plasmid construction in this study.

Plasmids	Primer name	Sequence	Features/purpose
pCAGGS_Influenza_NP	InfluenzaA_NP_f (*Kpn*I)	AGAATTCCTCGAG**GGTACC**ATCGAAATCATGGCGACCAAA	Derived from pCAGGS plasmid, continuously expression of Influenza A NP in cells
	InfluenzaA_NP_r (*Nhe*I)	GGAAAAAGATCT**GCTAGC**TTTCTTTAATTGTCGTACTCCTC	
pCAGGS_hCoV-NL63_N,	HCoVNL63_N_f(*Kpn*I)	AGAATTCCTCGAG**GGTACC**AATGGCTAATGTAAATTGGGC	Derived from pCAGGS plasmid, continuously expression of hCoV-NL63 N in cells
	HCoVNL63_N_r(*Nhe*I)	GGAAAAAGATCT**GCTAGC**AAAACAATTTAATGCAAAAC	
pCAGGS_hCoV-229E_N	HCoV229E_N_f(*Kpn*I)	AGAATTCCTCGAG**GGTACC**ACGAAAAGATGGCTACAGTC	Derived from pCAGGS plasmid, continuously expression of hCoV-229E N in cells
	HCoV229E_N_r(*Nhe*I)	GGAAAAAGATCT**GCTAGC**CATGTTTAGTTTACTTCATC	
pCAGGS_hCoV-OC43_N	HCoVOC43_N_f(*Kpn*I)	AGAATTCCTCGAG**GGTACC**TTAAGGATGTCTTTTACTCC	Derived from pCAGGS plasmid, continuously expression of hCoV-OC43 N in cells
	HCoVOC43_N_r(*Nhe*I)	GGAAAAAGATCT**GCTAGC**TTCTCTTATATTTCTGAGGT	
pCAGGS_hCoV-HKU1_N	HCoVHKU1_N_f(*Kpn*I)	AGAATTCCTCGAG**GGTACC**ATGGCATCCCCTGCTGCACC	Derived from pCAGGS plasmid, continuously expression of hCoV-HKU1 N in cells
	HCoVHKU1_N_r(*Nhe*I)	GGAAAAAGATCT**GCTAGC**CTAATCAGTGTTAACATCAAT	
pCAGGS_MERS_N	MERS_N_f(*Kpn*I)	AGAATTCCTCGAG**GGTACC**ATGTCTTATACTCCCGGTCA	Derived from pCAGGS plasmid, continuously expression of MERS N in cells
	MERS_N_r(*Nhe*I)	GGAAAAAGATCT**GCTAGC**TTAAGCAACAGAGTCTTCTAC	
pCAGGS_SARS-CoV-1_N	SARSCoV1_N_f(*Kpn*I)	AGAATTCCTCGAG**GGTACC**ATGTCTGATAATGGACCCCA	Derived from pCAGGS plasmid, continuously expression of SARS-CoV-1 N in cells
	SARSCoV1_N_r(*Nhe*I)	GGAAAAAGATCT**GCTAGC**TTATGCCTGAGTTGAATCAGC	
pCAGGS_SARS-CoV-2_N	SARSCoV2_N_f(*Kpn*I)	AGAATTCCTCGAG**GGTACC**CAAACTAAAATGTCTGATAATGGACCCC	Derived from pCAGGS plasmid, continuously expression of SARS-CoV-2 N in cells
	SARSCoV2_N_r(*Nhe*I)	GGAAAAAGATCT**GCTAGC**ATGAGTTTAGGCCTGAGTTGAGTCAGCA	
pFUSE_SARSCoV2_N	SARSCoV2_N_f(*Age*I)	AAA**ACCGGT**ATGTCTGATAATGGACCCCAAAATC	Derived from pFUSE-Fc plasmid, continuously expression of SARS-CoV-2 N in cells
	SARSCoV2_N_r (*Eco*RV)	AAAAA**GATATC**GGCCTGAGTTGAGTCAGCAC	
pFUSE_SARS-CoV-2_M	SARSCoV2_M_f (*Eco*RI)	AAAAA**GAATTC**ATGGCAGATTCCAACGGTACTATTACC	Derived from pFUSE-Fc plasmid, continuously expression of SARS-CoV-2 M protein in cells
	SARSCoV2_M_r(*Xho*I)	AAAAA**CTCGAGAC**CTGTACAAGCAAAGCAATATTGTC	
pFUSE_SARSCoV2_E	SARSCoV2_E_f(*Age*I)	AAA**ACCGGT**ATGTACTCATTCGTTTCGG	Derived from pFUSE-Fc plasmid, continuously expression of SARS-CoV-2 E protein in cells
	SARSCoV2_E_r (*Eco*RV)	AAAAA**GATATC**GACCAGAAGATCAGGAACTC	
pCAGGS_Lmut_EBOV plasmid	pCAGGS_EBOV_L_F (*Kpn*I)	AGAATTCCTCGAG**GGTACC**ATGTTCATGCCTTCTTCT	Derived from the pCAGGS plasmid, the functional L was substituted with the inactive mutant L.
	pCAGGS_ EBOV_L _R (*Nhe*I)	GGAAAAAGATCT**GCTAGC**TTATCAATCAAACCTGTAGAG	
	EBOV_Lmut_Link (GAAAmotif)_F	ATGGGTGCAGCAGCATGCATTACTGTTTTATCA	
	EBOV_Lmut_Link (GAAAmotif)_R	GCATGCTGCTGCACCCATCACAGCTGAGCG	

Restriction enzyme sites used are underlined.

(HCoV)-OC43, HCoV-229E, HCoV-HKU1, MERS, SARS-CoV-1, SARS-CoV-2, and the sequence of nucleocapsid protein (NP) gene of the influenza A/WSN/33 virus (influenza A) were chemically synthesized (Genomics, Taiwan). The N or NP DNA fragments were generated through PCR amplification, and the sequences of the primer sets employed for cloning are meticulously detailed in Table 1. To generate a series of recombinant plasmids, the amplified N or NP DNA fragments were cloned into the pCAGGS plasmid, which had been pre-digested with *Kpn*I and *Nhe*I restriction enzymes (NEB, Ipswich, MA, USA). To elucidate the role of the N protein in the EBOV MiniG system, an EBOV-L polymerase mutant was engineered by modifying the catalytic center of the EBOV-L gene, changing the GDNQ motif to a GAAA motif [15]. This modification was achieved through a combination of conventional and overlap-extension PCR methods. We initially performed two separate touchdown PCRs, utilizing Phusion High-Fidelity DNA polymerase (Thermo Fisher Scientific Inc., Boston, MA, USA) with pCAGGS-L serving as the template. The first PCR was conducted with primers pCAGGS_EBOV_L_F(*Kpn*I) and EBOV_Lmut_Link(GAAAmotif)_R, while the second PCR employed primers EBOV_Lmut_Link(GAAAmotif)_F and pCAGGS_EBOV_L_R(*Nhe*I). A subsequent PCR was executed using the amplicons from the initial PCRs as templates, along with primers pCAGGS_EBOV_L_F(*Kpn*I) and pCAGGS_EBOV_L_R(*Nhe*I). The resulting PCR product, embodying the L mutation, was then skillfully incorporated into a pre-digested pCAGGS plasmid using *Kpn*I and *Nhe*I restriction enzymes. This intricate procedure culminated in the generation of a specialized construct, which we have designated as pCAGGS_Lmutant plasmid. The DNA sequences of the SARS-CoV-2 membrane protein (M), envelope protein (E), and N were cloned into the pFUSE-mIgG2a-Fc1 expression vector (Invitrogen, Waltham, MA, USA).

2.3. Measuring the minigenome activity

The experimental design is illustrated in Fig. 1. The proportion of plasmids used in the EBOV MiniG system has been adjusted from the proportions reported in the previously published study [15]. Based on our pilot study, we discerned that elevating the concentration of the VP35 plasmid notably amplifies the signal output of the MiniG system. The EBOV MiniG system used for transfection contained the following: the EBOV minigenome (1.5 μg), pCAGGS_L_EBOV (1 μg), the pCAGGS_NP_EBOV (0.25 μg), pCAGGS_VP35_EBOV (0.75 μg) and pCAGGS_VP30 (0.25 μg). To transfect the HEK293T cells, T-Pro Non-liposome transfection Reagent II (Genestar biotechnology, Kaohsiung, Taiwan) was used according to the manufacturer's recommendations. HEK293T cells were co-transfected with the EBOV MiniG system and different expression plasmids. For each experimental batch, we included a blank group to eliminate any background noise originating from the cells. Additionally, a negative control was established by transfecting with the EBOV MiniG system with the pCAAGS_Lmutant plasmid. To ensure accurate monitoring of the transfection efficiency, a control group was included in every experiment. In this control group, HEK293T cells were transfected with 500 ng of a plasmid known as pGFP-N2 (Addgene, Watertown, MA, USA) solely expressing the GFP protein. The signal intensity for each positive control batch was required to fall within the range of 50–70 %. After transfection, the minigenome activity was analyzed by examining the number of GFP-positive cells using a CytoFLEX flow cytometer (Beckman Coulter Inc., Brea, CA, USA) and a BS-7000 series fluorescence microscope (Beijing BestScope Technology Co., Ltd., China). The percentage of GFP-positive cells was analyzed using FlowJo 10.0.7 R2 (Tree Star, Ashland, OR, USA). The GFP protein expression was detected using western blotting. Unless otherwise specified, all analyses were conducted at a time point of 48 h post-transfection.

2.4. Western blot

The cells were lysed using Radioimmunoprecipitation assay (RIPA) buffer (Sigma-Aldrich, Burlington, MA, USA) supplemented with protease inhibitors (Merck Millipore, Billerica, MA, USA). The proteins in the protein lysates were quantified and subjected to SDS-PAGE, followed by electroblotting onto a PVDF membrane. Membranes were incubated with the Mouse Anti-Green Fluorescent Protein Antibody, (1:1000 dilution) (Sigma-Aldrich, Burlington, MA, USA), Rabbit anti-EBOV L-Polymerase pAb, (1:5000 dilution), (IBT Bioservices, Rockville, MD, USA) and Mouse anti-glyceraldehyde-3-phosphate dehydrogenase (GAPDH) antibodies, (1:5000 dilution) (GeneTex, Irvine, CA, USA). The reactive bands were visualized using chemiluminescence detection reagents (Merck

Table 2
Primers used in this study.

Primer name	Sequence (5'to 3')	Features/purpose
qPCR_eGFP_f	ACGTAAACGGCCACAAGTTC	Quantitative of the GFP transcripts
qPCR_eGFP_r	AAGTCGTGCTGCTTCATGTG	
qPCR_GAPDH _f	GTCTCCTCTGACTTCAACAGCG	Quantitative of the GAPDH transcripts
qPCR_GAPDH_r	ACCACCCTGTTGCTGTAGCCAA	
EBoVmg_vRNA(RT)_F	**GGCCGTCATGGTGGCGAAT**-GCTACCCCGACCACATGAAG	Reverse transcription of vRNA
EBoVmg_cRNA(RT)_R	**GCTAGCTTCAGCTAGGCATC**-CTTGTACAGCTCGTCCATGC	Reverse transcription of cRNA
EBoVmg_mRNA(RT)_R	**CCAGATCGTTCGAGTCGT**-TTTTTTTTTTTTTTTTTTTT	Reverse transcription of mRNA
EBoVmg_vRNA(QPCR)_F	GGCCGTCATGGTGGCGAAT	Quantitative of vRNA
EBoVmg_vRNA(QPCR)_R	CGGGTCTTGTAGTTGCCGT	
EBoVmg_cmRNA(QPCR)_F	TGAGCAAAGACCCCAACGAG	Quantitative of cRNA
EBoVmg_cRNA(QPCR)_R	GCTAGCTTCAGCTAGGCATC	
EBoVmg_cmRNA(QPCR)_F	TGAGCAAAGACCCCAACGAG	Quantitative of mRNA
EBoVmg_mRNA(QPCR)_R	CCAGATCGTTCGAGTCGT	

The bottom line is the tag.

Millipore, Billerica, MA, USA).

2.5. Real-time quantitative PCR

The total RNA was extracted from the infected cells using TRIzol reagent (Thermo Fisher Scientific Inc., Boston, MA, USA). Reverse transcription (RT) was performed using the SuperScript IV First-Strand Synthesis System (Thermo Fisher Scientific Inc., Boston, MA, USA). Quantitative PCR was performed using the SYBR Green PCR Master Mix (Thermo Fisher Scientific Inc., Boston, MA, USA). All the primers used are listed in Table 2. The transcription levels of total transcripts, mRNA, vRNA, cRNA, and the *GAPDH* gene were measured via RT-qPCR using a LightCycler 480 II instrument (Roche Diagnostics GmbH, Mannheim, Germany). For the accurate quantification of gene expression, the genes were cloned into the pGEM-T Easy vector (Promega, Madison, WI, USA), and a standard curve was constructed as previously described [21]. The target gene and *GAPDH* copy numbers in the sample were assessed by comparing the sample threshold cycle values to a standard curve and were expressed in $\log_{10}$(copies of transcripts per 10^5 copies of *GAPDH*). Tagged RT quantitative PCR was used to differentiate and quantify the three types of viral RNA, as previously reported [8, 22]. cDNA synthesis was performed using "tagged" primers complementary to each type of RNA. Amplified cDNA was quantified via

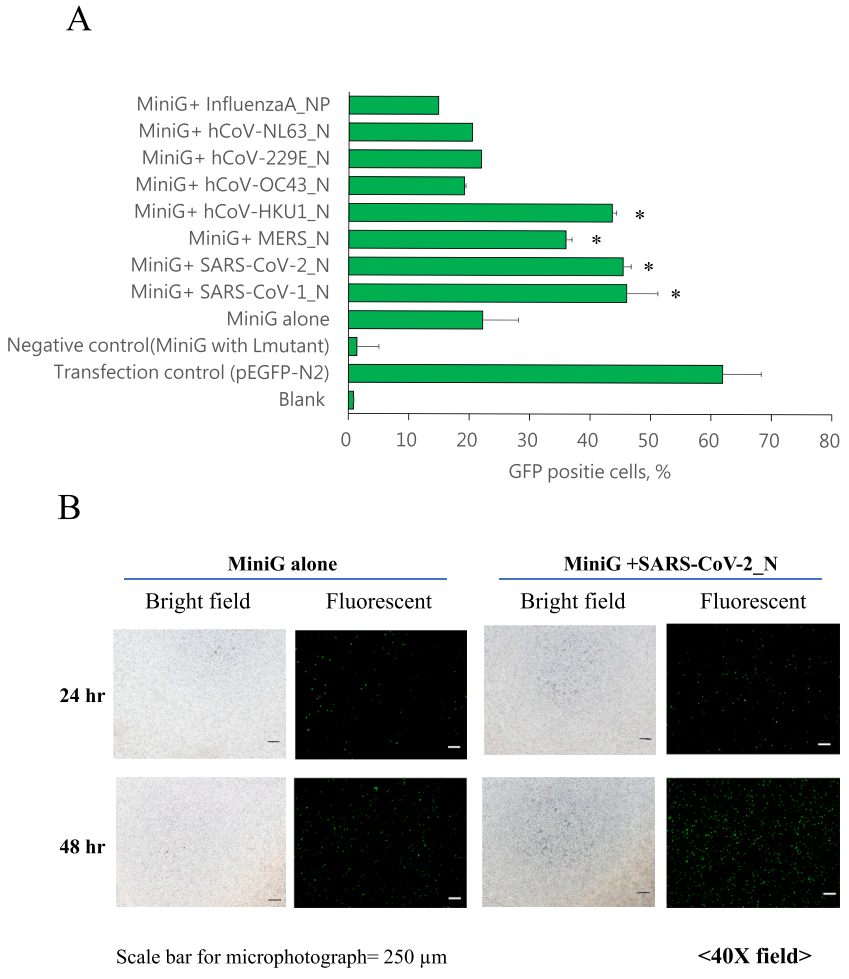

Fig. 2. HCoV nucleocapsid protein (N) increases the ratio of GFP-positive cells in the EBOV MiniG system. (A). The GFP-positive cells in the HEK293T cells transfected with the EBOV MiniG system alone or together with various plasmids expressing the N at 48 h. Blank: Consists solely of HEK293T cells to eliminate any cellular background noise. Negative control: Features the MiniG system transfected with the pCAGGS-EBOV-L mutant plasmid to account for non-specific effects. Transfection control: Utilizes pEGFP-N2 as a marker to monitor the efficiency of the transfection process. (B) Fluorescence microscopy showing the HEK293T cells transfected using the EBOV MiniG system alone or together with the pCAGG_SARS-CoV-2 N at 24 h and 48 h post-transfection. Scale bar for the microphotograph is 250 μm (C) Flow cytometry analysis of the EBOV MiniG system alone (green) or with the pCAGG_SARS-CoV-2 N (red). Left graph: 24 h post-transfection; right graph: 48 h post-transfection. (D) The percentage of GFP-positive cells among the HEK293T cells transfected with the EBOV MiniG system alone or together with the pCAGG_SARS-CoV-2 N. (E) Western blot of the GFP and GAPDH proteins in the HEK293T cells transfected with the EBOV MiniG system alone or together with the pCAGG_SARS-CoV-2 N. The uncropped Western blot is in supplementary figure S1 (F) The Western blot quantification results. The data represent the mean and standard deviations (SD) of three independent experiments (*, $P < 0.05$; Mann-Whitney test).

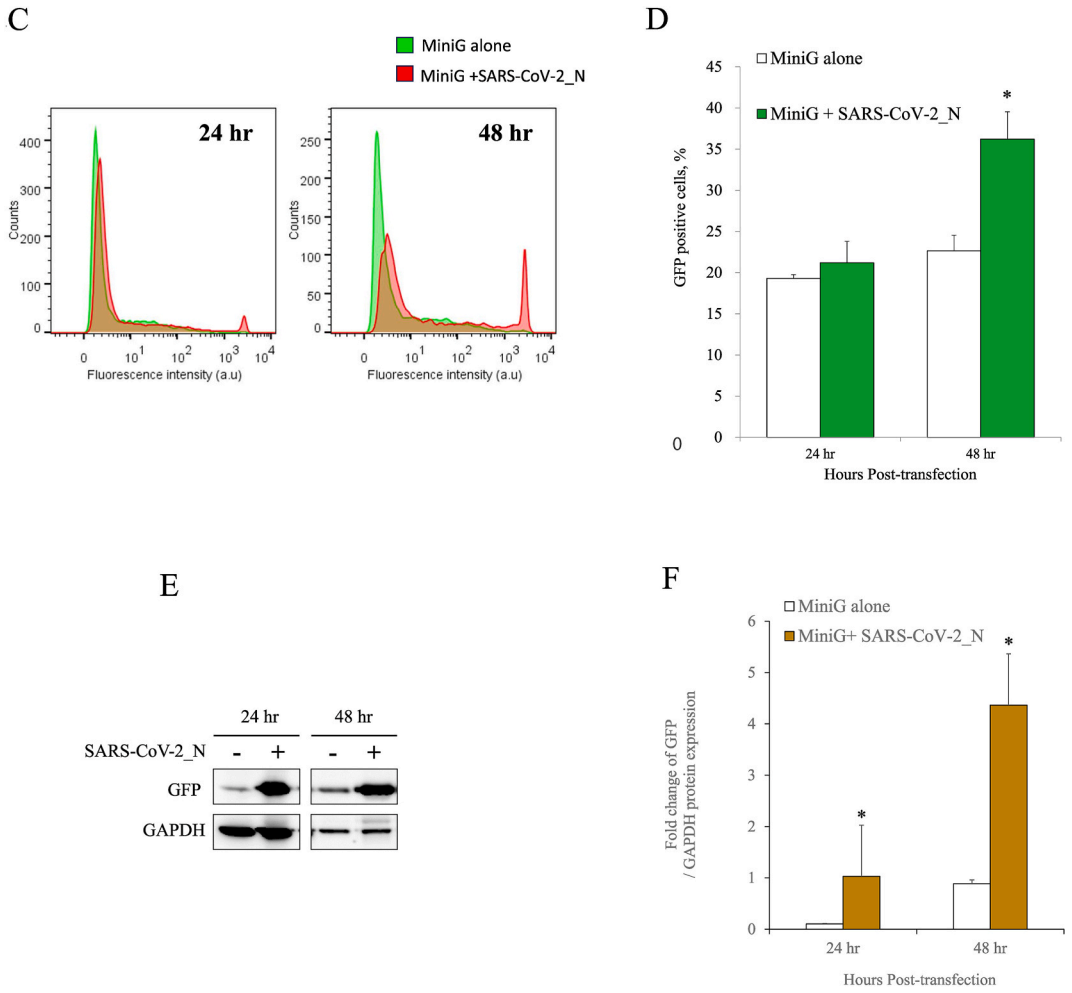

Fig. 2. (*continued*).

real-time PCR using segment-specific primer sets.

2.6. Determining the half-maximal effective concentration

Remdesivir and rupintrivir were sourced from Sigma-Aldrich (Burlington, MA, USA). Following a 6-h incubation period post-transfection with either the EBOV MiniG or EBOV MiniG Plus system, HEK293T cells were treated with serially diluted concentrations of remdesivir and rupintrivir, ranging from 0 to 800 nM, in a 2-fold dilution series. After a 48-h incubation period, the cells were collected and analyzed using flow cytometry, as described above. These experiments were performed thrice, and each dilution was assayed in triplicate. At high antiviral drug concentrations, GFP-expressing cells weakly inhibited by the drug were sensitively detected by flow cytometry. Therefore, 50 % effective concentration (EC50) calculation was defined as the drug concentration that reduced the number of GFP cells by half [23,24].

2.7. Z-factor calculation

Z-factor values were calculated to compare the MiniG Plus system with the MiniG system as delineated in a previous publication [25]. In the positive control, all components of the MiniG or MiniG Plus system were present, while the negative control included all components of the MiniG system along with the pCAAGS_Lmutant plasmid.

2.8. Data analysis

Statistical analysis was performed using SPSS version 20.0 (SPSS Inc., IBM Company, Chicago, Ill, USA) and the statistical differences among various groups were calculated using the Mann-Whitney test. Differences were considered statistically significant at a

$P < 0.05$.

3. Results

3.1. The nucleocapsid proteins of human coronaviruses increase the ratio of GFP-positive cells in the EBOV MiniG system

A total of 48 h after transfection, the ratio of GFP-positive cells transfected using the EBOV MiniG system alone was 22.2 % ± 0.1 % (Fig. 2A). Interestingly, the co-transfection of cells with plasmids expressing the Ns from SARS-CoV-1, SARS-CoV-2, MERS, and HKU1 and with the EBOV MiniG system significantly increased the ratio of GFP-positive cells by 2.1- (46 % ± 6.4 %), 2.0- (45.4 % ± 3.6 %), 1.6- (35.9 % ± 5.9 %), and 2.0-fold (43.6 % ± 5.2 %), respectively. To investigate this boosting effect, the follow-up studies focused on comparing the effects of SARS-CoV-2 N on the EBOV MiniG system 24 and 48 h post-transfection. According to the flow cytometry and microscopy results, the SARS-CoV-2 N not only increased the ratio of GFP-positive cells but also enhanced their fluorescence intensity

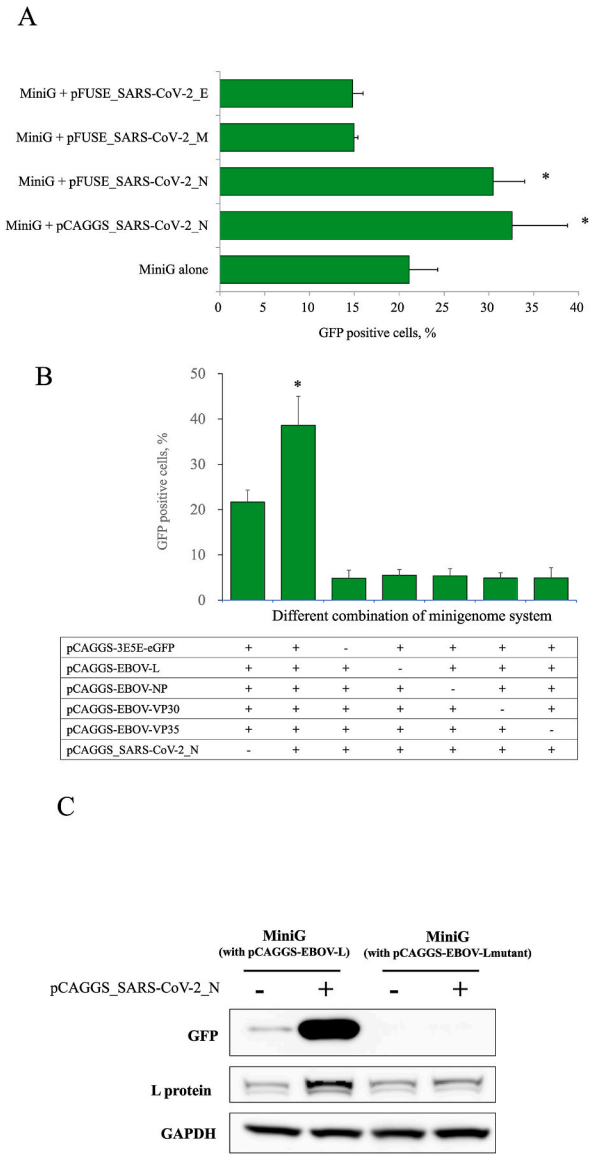

Fig. 3. The SARS-CoV-2 N increases the proportion of GFP-positive cells in the complete EBOV MiniG system. (A) The percentage of GFP-positive cells at 48 h in the HEK293T cells transfected with the EBOV MiniG system alone or together with the pCAGGS-based plasmid or the pFUSE-based plasmid. (B) The interaction of the SARS-CoV-2 N with the EBOV MiniG system (minigenome system, VP35, VP30, NP, and L). The data represent the mean and standard deviations (SDs) of three independent experiments (*, $P < 0.05$; Mann-Whitney test). (C) Western blot analysis was conducted on HEK293T cells transfected with the EBOV MiniG system (using either pCAGGS-EBOV-L or pCAGGS-EBOV-L mutant) alone or together with the pCAGG_SARS-CoV-2 N plasmid. The uncropped Western blot is in Supplementary Fig. S2.

(Fig. 2B and C). As shown in Fig. 2D, the proportion of GFP-positive cells in the EBOV MiniG system with SARS-CoV-2 N was significantly higher than that in the EBOV MiniG system with no N by approximately 1.6-fold at 48 h after transfection ($P < 0.05$). The Western blot analysis results confirmed that the accumulation of GFP protein was time-dependent (Fig. 2E). Upon comparing the MiniG system supplemented with the SARS-CoV-2 N protein to the MiniG system without it, a 4.9-fold increase in the relative quantity of GFP protein compared to GAPDH was observed 48 h post-transfection (Fig. 2F). These results indicate that the Ns of coronaviruses affect the GFP expression in the EBOV MiniG system.

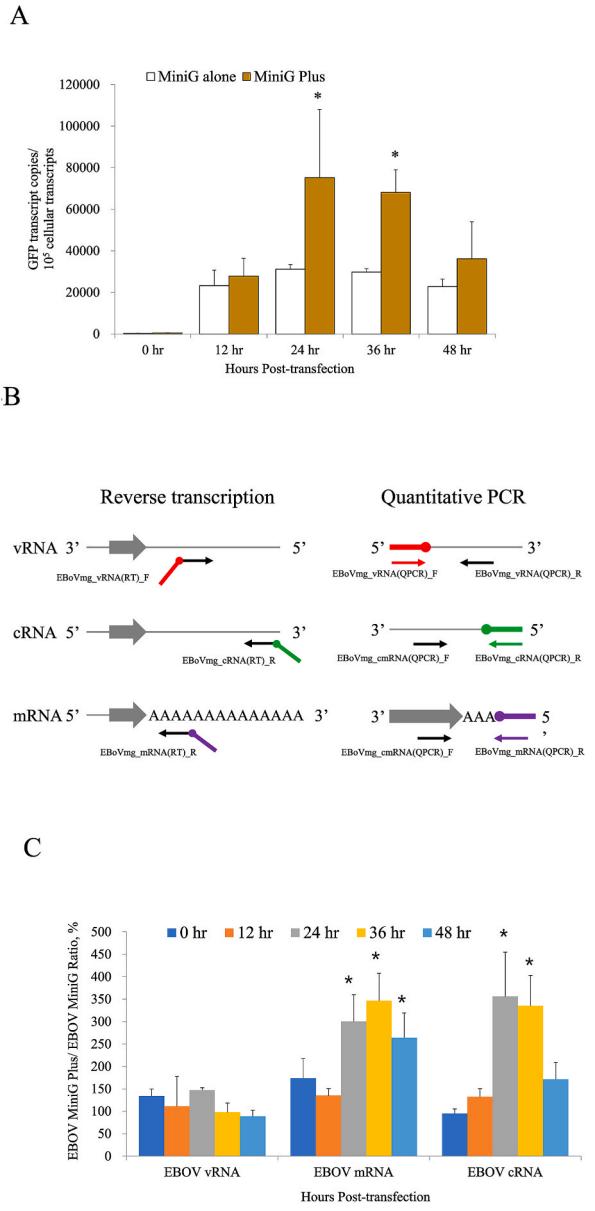

Fig. 4. Kinetics of the transcripts in the EBOV MiniG system alone and in the MiniG Plus system. (A) Comparison of the GFP transcripts between the EBOV MiniG system alone (MiniG alone) and the system with the SARS-CoV-2 N (MiniG Plus). (B) Schematics of the tagged RT quantitative PCR steps. Reverse transcription is performed using "tagged" primers complementary to each type of RNA. A tag of 18–20 nt unrelated to the minigenome, is shown as red, green, and purple bars for the vRNAtag, cRNAtag, and mRNAtag, respectively. The tagged cDNA was amplified via PCR using the tag portion of the cDNA primer as the forward primer and a segment-specific oligonucleotide as the reverse primer. (C) Comparison of the levels of mRNA, cRNA, and vRNA between the MiniG alone and the MiniG Plus for the indicated times. The data represent the mean and standard deviations (SD) of three independent experiments (*, $P < 0.05$; Mann-Whitney test)

3.2. The contribution of SARS-CoV-2 N in the EBOV MiniG system

To confirm the role of SARS-CoV-2 N in the EBOV MiniG system, the plasmid backbone was changed from a pCAGGS-based plasmid to a pFUSE-based plasmid. As shown in Fig. 3A, the N of SARS-CoV-2 significantly increased the proportion of GFP-positive cells in the EBOV MiniG system ($P < 0.05$), whereas the M and E proteins did not. The ratio of GFP-positive cells increased significantly only in the

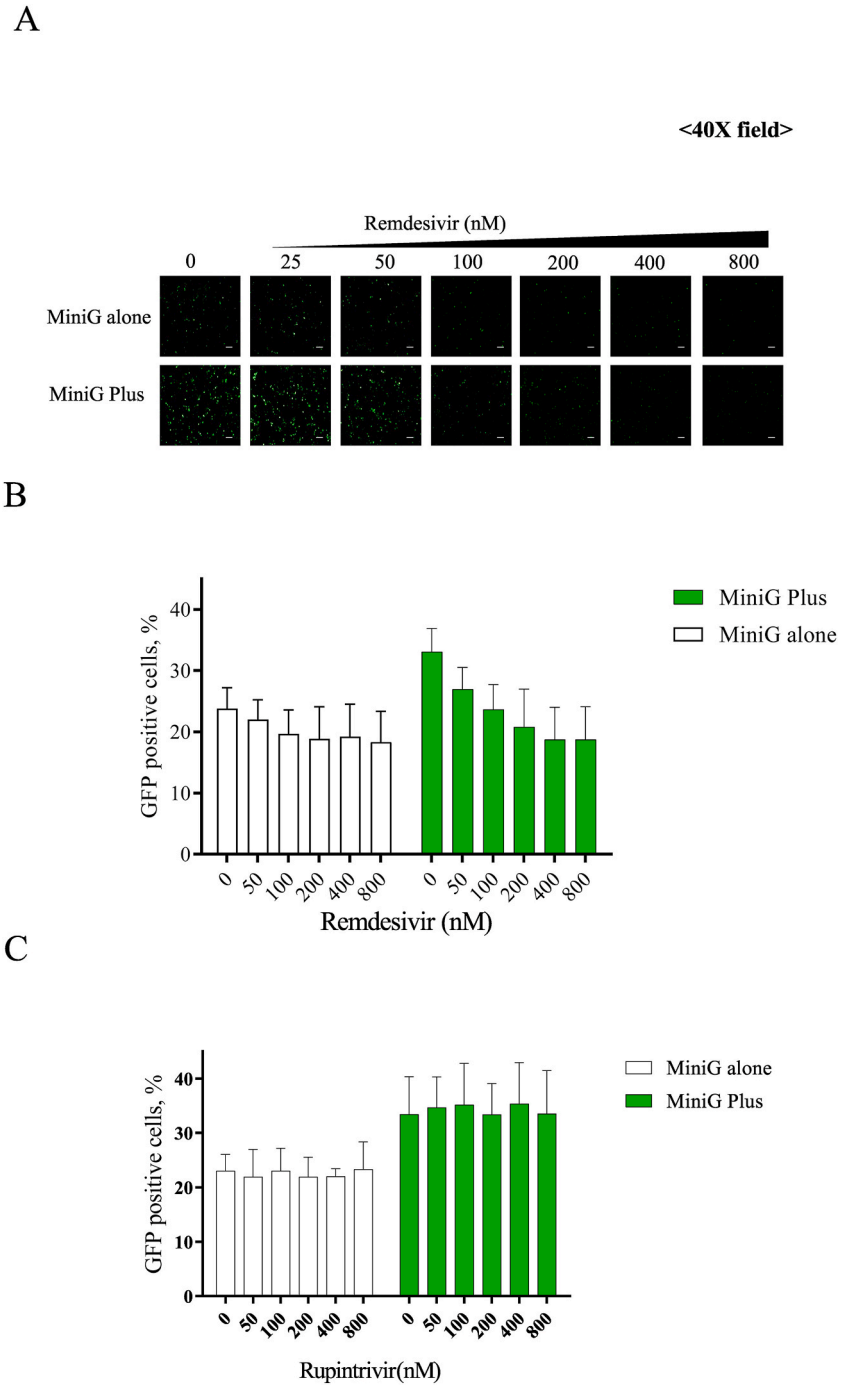

Fig. 5. Comparison between the antiviral drug screening performance of the MiniG system alone and the MiniG Plus system. (A) Fluorescence micrographs of the EBOV MiniG system alone and the MiniG Plus system treated with serial dilutions of remdesivir or dimethyl sulfoxide (control) taken 48 h post-transfection. Scale bar of the microphotographs is 250 μm. (B) The effect of remdesivir on the EBOV MiniG system alone and on the MiniG Plus system. (C) The effect of rupintrivir on the EBOV MiniG system alone and on the MiniG Plus system.

presence of SARS-CoV-2 N with all five plasmids in the EBOV MiniG system ($P < 0.05$) (Fig. 3B). Regardless of whether N was present, the expression of the GFP protein was extinguished once the wild-type L plasmid (pCAGGS-EBOV-L) within the MiniG system was replaced with the L mutant plasmid (pCAGGS-EBOV-Lmutant) This confirmed that N can function as a transcriptional activator only when the mechanisms of the MiniG system are intact (Fig. 3C).

3.3. The transcript dynamics in the EBOV MiniG and EBOV MiniG plus systems

We subsequently mixed the plasmids expressing SARS-CoV-2 N in the EBOV MiniG system and named it as EBOV MiniG Plus system. Compared with that of the EBOV MiniG system, the GFP transcript level of the EBOV MiniG Plus system was significantly increased 24 h after transfection ($P < 0.05$) (Fig. 4A). The levels of the three types of minigenomic RNA (mRNA, vRNA, and cRNA) were assessed separately using tagged RT quantitative PCR (Fig. 4B). As shown in Fig. 4C, the mRNA and cRNA levels of the EBOV MiniG Plus system were three times higher than those of the EBOV MiniG system 24 h after transfection.

3.4. The EBOV MiniG plus system as a powerful tool for antiviral drug screening

In an effort to assess the suitability of the EBOV MiniG Plus system for antiviral drug screening assays, we initially calculated the Z-factor to enable a direct comparison with the existing MiniG system. The Z-factor values obtained were 0.72 for the MiniG Plus system and 0.52 for the MiniG system. These metrics clearly indicate that the MiniG Plus system is significantly better suited for high-throughput screening applications. Subsequently, to further validate the system's applicability in antiviral drug screening, two known antiviral drugs, remdesivir and rupintrivir, were selected for evaluation. Remdesivir works by inhibiting the EBOV's RNA-dependent RNA polymerase, directly curtailing the functionality of the EBOV MiniG system. Contrarily, rupintrivir, a 3C protease inhibitor, is employed as a specific control in this study, as it does not selectively obstruct any part of the EBOV's replication process. Dose-dependent inhibition assays were performed using the MiniG system and the MiniG Plus system, and their respective EC50 values were measured and compared based on the proportion of GFP-positive cells. Remdesivir effectively inhibited the activity of the GFP-positive cells in both systems in a dose-dependent manner (Fig. 5A and B). Under remdesivir (0–800 nm), the inhibition of GFP-positive cells in the MiniG Plus system (33.1%–18.7 %) was more significant than the MiniG system (23.8%–18 %). The EC50 values of remdesivir in the MiniG and MiniG Plus systems were 86.95 nM (53.1–173.5 nM) and 83.99 nM (65.5–110.9 nM), respectively. Rupintrivir, a protease inhibitor, had no inhibitory effect on either system at any of the concentrations tested (Fig. 5C).

4. Discussion

In the initial phase of our research, our attention was centered on evaluating the influence of the N protein derived from RNA viruses on the operational efficacy of the MiniG system. Unexpectedly, we unearthed a pivotal role for the N protein from Coronaviruses: it markedly enhances plasmid transcription. This serendipitous discovery compelled us to incorporate the N protein into our minigenome system, where it serves as a potent activator, significantly amplifying the signal output of the MiniG system. The N protein is the most abundant structural protein in coronaviruses that binds to genomic RNA and is a promising target for diagnostic detection and antiviral drug design [17,18,20,26,27]. In our study, the introduction of specific N proteins from SARS-CoV-1, SARS-CoV-2, MERS, and HKU1 resulted in a marked increase in the proportion of fluorescent cells, with fold increases ranging from 1.6 to 2.1. Furthermore, the expression of these N proteins led to a noticeable surge in the fluorescence intensity of GFP-positive cells within the context of the EBOV MiniG system. Comparing the protein identities of the Ns of SARS-CoV-1, MERS, and HKU1 to that of SARS-CoV-2 (100 %), they were 91 %, 48 %, and 37 %, respectively. Interestingly, the Ns of SARS-CoV-1 and SARS-CoV-2 showed highly conserved structures and demonstrated the highest enhancement effects (46 % and 45 %, respectively). The structure of the N in human coronaviruses is conserved, comprising two independently folded domains, the N-terminal domain (NTD) and the C-terminal domain (CTD), which are connected by an intrinsically disordered region [19,20,26–28]. The NTD is responsible for RNA binding, while the CTD is responsible for dimerization. The intrinsically disordered region plays a crucial role in regulating the activity of both the NTD and CTD [20]. Both NTDs and CTDs have a high affinity for RNA and DNA [19,26]. Therefore, it is necessary to identify the key motifs of coronavirus Ns responsible for promoting RNA expression in future research.

Here, we observed a 3-fold increase in the cRNA and mRNA levels 24 h post-transfection in the presence of SARS-CoV-2 Ns using tagged quantitative real-time RT-PCR. This is the first time that viral proteins other than EBOV have been found to stimulate the expression of the EBOV MiniG system. According to previous studies, the overexpression of VP40 and VP24 downregulates the expression of the EBOV MiniG system [8,10]. VP24 can interact with two proteins in the RNP complex, NP and VP35, which directly inhibit the RNP complex, resulting in a simultaneous decrease in the production of these three RNAs [28,29]. However, VP40 has been discovered to suppress the expression of both mRNA/cRNA and vRNA [29]. These findings not only suggest that these two proteins have different mechanisms of inhibiting the EBOV MiniG system, but also imply that the system can be directly or indirectly regulated by other factors. In our study, we observed that the presence of SARS-CoV-2 N protein resulted in increased reporter gene activity only when all the components of the RNP complex were intact. Based on these findings, we propose that SARS-CoV-2 N acts as an independent activator, enhancing the expression mechanism of the EBOV MiniG system. Our research suggests that the SARS-CoV-2 N protein acts as a transcription activator within the MiniG system. Detailed evaluation of this mechanism will be the focus of our forthcoming studies.

One of the primary applications of minigenome systems is antiviral compound screening [8,24,30]. Luciferase is the most commonly used reporter gene in antiviral compound screening systems because of its high sensitivity [24,31]. Unlike luciferase, which

requires a substrate to generate a signal, GFP has the advantage of being directly detectable by fluorescence microscopy or flow cytometry. In a previously published MiniG system used for drug screening in a 96-well format, a luciferase system was employed for quantitative measurements [15]. However, luciferase assays require additional enzyme extraction steps, which, although accurate, are time-consuming and increase costs. In our study, we observed an enhancement of the GFP signal in the presence of the N protein within the Minigenome system. Therefore, the MiniG Plus system allows direct application of the GFP system for drug screening. This ultimately enables live cell measurements of GFP, reduces the level of operational complexity, and offers the potential for an automated image screening system.

Our study found that the drug efficacy can be directly observed and compared in the EBOV MiniG Plus system, which has the potential to develop into a high-throughput screening system. Remdesivir is known to specifically inhibit the RNA-dependent RNA polymerase, thus demonstrating antiviral efficacy against both Ebola virus and SARS-CoV-2. Importantly, Remdesivir does not act on the SARS-CoV-2 N protein. Therefore, our MiniG Plus system is optimally designed for screening antiviral drugs that specifically target the replication mechanisms of the Ebola virus [32,33]. In the inhibition experiment with remdesivir, the EC50 values of the EBOV MiniG and the EBOV MiniG Plus systems were similar. Compared to the MiniG system, the MiniG Plus system possesses a higher initial GFP-positive value, allowing for more distinct detection of variations influenced by remdesivir. The use of the infectious EBOV in different cell lines showed that remdesivir has EC50 values ranging from 10 nM to 100 nM [30]. However, the EC50 value was 420 nM in a minigenome assay [34]. This difference may be because in small genome systems there are more RNP complexes depending on the number of expression plasmids transfected, which may require higher levels of remdesivir to affect polymerase activity. Our data clearly supports the efficacy of remdesivir. Most importantly, the EBOV MiniG Plus system could increase the fluorescent signal without affecting the EC50 value of the drug.

To confirm that the activator function of SARS-CoV-2 N is independent of the expression vector, we employed different vectors and observed consistent activity. In HEK293T cells, the complete SARS-CoV-2 N was derived from the CMV promoter on the pCAGGS plasmid. However, the pFUSE-Fc plasmid contains a hEF1-HTLV promoter that expresses a fusion protein, which is a SARS-CoV-2 N-mouse IgG Fc fusion protein. We found that the SARS-CoV-2 N promoted the EBOV MiniG system, regardless of its expression in either plasmid system. Minigenome systems have been developed as platforms to screen potential antiviral drugs that interfere with the viral transcription and replication processes of many high-risk viruses other than the EBOV, such as the Marburg virus [35], severe fever with thrombocytopenia syndrome virus [36], Rift Valley fever virus [37], Nipah virus [38] Crimean-Congo hemorrhagic fever virus [39], Hantaan virus [40] and SARS-CoV-2 [38]. We believe that this model can be utilized in other minigenome systems to enhance their activity and increase the reliability of the results obtained.

To our knowledge, this is the first time that the human coronavirus N was shown to act as an activator in the EBOV MiniG system. The EBOV MiniG Plus system had a higher ratio of GFP-positive cells than the EBOV MiniG system, thus resulting in a more effective drug screening. Finally, we believe that this application is not limited to the EBOV MiniG system, but that it can also be applied to other minigenome systems and may constitute a useful tool for screening antiviral drugs that inhibit the viral replication of high-risk viruses under BSL-2 conditions.

Funding statement

This work was supported by grants from the Ministry of National Defense, R.O.C. (MND-MAB-D-113172, MND-MAB-C04-112016, MND-MAB-D-111104 and MND-MAB-110065) and the National Science and Technology Council in Taiwan (NSTC 112-2320-B-016-007; NSTC 111-2320-B-016-014, NSTC 111-2321-B-016-002 and NSTC 111-2740-B-016 -001)

Data availability statement

All data included in the article. The essential materials supporting this article will be shared on reasonable request to the corresponding author.

CRediT authorship contribution statement

Chi-Ju Hsu: Conceptualization, Data curation, Project administration. **Cheng-Hsiu Chen:** Data curation, Methodology, Resources. **Wen-Ting Chen:** Validation. **Ping-Cheng Liu:** Methodology, Resources. **Tein-Yao Chang:** Formal analysis. **Meng-He Lin:** Validation. **Cheng-Cheung Chen:** Formal analysis. **Hsing-Yu Chen:** Conceptualization, Writing – original draft. **Chih-Heng Huang:** Formal analysis. **Yun-Hsiang Cheng:** Data curation, Formal analysis, Writing – original draft, Writing – review & editing. **Jun-Ren Sun:** Conceptualization, Data curation, Funding acquisition, Investigation, Project administration, Resources, Writing – original draft, Writing – review & editing.

Declaration of competing interest

The authors declare that they have no known competing financial interests or personal relationships that could have appeared to influence the work reported in this paper.

Acknowledgements

The authors wish to thank Prof. E. Mühlberger, Boston University, MA, USA for providing the EBOV minigenome system. The authors also wish to thank the technical services provided by the core facility platform for emerging infectious disease research of the National Core Facility for Biopharmatheuticals, Ministry of Science and Technology, Taiwan.

Appendix A. Supplementary data

Supplementary data to this article can be found online at https://doi.org/10.1016/j.heliyon.2023.e22138.

References

[1] A.D.J. Korath, J. Janda, E. Untersmayr, M. Sokolowska, W. Feleszko, I. Agache, et al., One Health: EAACI Position Paper on coronaviruses at the human-animal interface, with a specific focus on comparative and zoonotic aspects of SARS-CoV-2, Allergy 77 (1) (2022) 55–71, https://doi.org/10.1111/all.14991.
[2] B. Hu, H. Guo, P. Zhou, Z.L. Shi, Characteristics of SARS-CoV-2 and COVID-19, Nat. Rev. Microbiol. 19 (3) (2021) 141–154, https://doi.org/10.1038/s41579-020-00459-7.
[3] A.C. Brant, W. Tian, V. Majerciak, W. Yang, Z.M. Zheng, SARS-CoV-2: from its discovery to genome structure, transcription, and replication, Cell Biosci. 11 (1) (2021) 136, https://doi.org/10.1186/s13578-021-00643-z.
[4] J. Pekar, M. Worobey, N. Moshiri, K. Scheffler, J.O. Wertheim, Timing the SARS-CoV-2 index case in Hubei province, Science 372 (6540) (2021) 412–417, https://doi.org/10.1126/science.abf8003.
[5] C.B. Levine, C.E. Mire, T.W. Geisbert, Comparison of Zaire and Bundibugyo Ebolavirus polymerase complexes and susceptibility to antivirals through a newly developed Bundibugyo minigenome system, J. Virol. 95 (20) (2021), e0064321, https://doi.org/10.1128/JVI.00643-21.
[6] K.B. Yeh, K. Tabynov, F.K. Parekh, I. Mombo, K. Parker, K. Tabynov, et al., Significance of high-containment biological laboratories performing work during the COVID-19 pandemic: biosafety level-3 and -4 labs, Front. Bioeng. Biotechnol. 9 (2021), 720315, https://doi.org/10.3389/fbioe.2021.720315.
[7] A.M. Kaufer, T. Theis, K.A. Lau, J.L. Gray, W.D. Rawlinson, Laboratory biosafety measures involving SARS-CoV-2 and the classification as a Risk Group 3 biological agent, Pathology 52 (7) (2020) 790–795, https://doi.org/10.1016/j.pathol.2020.09.006.
[8] W. Tao, T. Gan, M. Guo, Y. Xu, J. Zhong, Novel stable Ebola Virus minigenome replicon reveals remarkable stability of the viral genome, J. Virol. 91 (22) (2017), https://doi.org/10.1128/JVI.01316-17.
[9] K. Wing, S. Oza, C. Houlihan, J.R. Glynn, S. Irvine, C.E. Warrell, et al., Surviving Ebola: a historical cohort study of Ebola mortality and survival in Sierra Leone 2014-2015, PLoS One 13 (12) (2018), e0209655, https://doi.org/10.1371/journal.pone.0209655.
[10] E. Muhlberger, M. Weik, V.E. Volchkov, H.D. Klenk, S. Becker, Comparison of the transcription and replication strategies of marburg virus and Ebola virus by using artificial replication systems, J. Virol. 73 (3) (1999) 2333–2342, https://doi.org/10.1128/JVI.73.3.2333-2342.1999.
[11] T. Hoenen, A. Groseth, J. Callison, A. Takada, H. Feldmann, A novel Ebola virus expressing luciferase allows for rapid and quantitative testing of antivirals, Antiviral Res 99 (3) (2013) 207–213, https://doi.org/10.1016/j.antiviral.2013.05.017.
[12] M.R. Edwards, C. Pietzsch, T. Vausselin, M.L. Shaw, A. Bukreyev, C.F. Basler, High-throughput minigenome system for identifying small-molecule inhibitors of Ebola virus replication, ACS Infect. Dis. 1 (8) (2015) 380–387, https://doi.org/10.1021/acsinfecdis.5b00053.
[13] N. Lee, D. Shum, A. Konig, H. Kim, J. Heo, S. Min, et al., High-throughput drug screening using the Ebola virus transcription- and replication-competent virus-like particle system, Antiviral Res 158 (2018) 226–237, https://doi.org/10.1016/j.antiviral.2018.08.013.
[14] T. Hoenen, A. Groseth, F. de Kok-Mercado, J.H. Kuhn, V. Wahl-Jensen, Minigenomes, transcription and replication competent virus-like particles and beyond: reverse genetics systems for filoviruses and other negative stranded hemorrhagic fever viruses, Antiviral Res 91 (2) (2011) 195–208, https://doi.org/10.1016/j.antiviral.2011.06.003.
[15] E.V. Nelson, J.R. Pacheco, A.J. Hume, T.N. Cressey, L.R. Deflube, J.B. Ruedas, et al., An RNA polymerase II-driven Ebola virus minigenome system as an advanced tool for antiviral drug screening, Antiviral Res 146 (2017) 21–27, https://doi.org/10.1016/j.antiviral.2017.08.005.
[16] J. Su, Y. Dou, Y. You, X. Cai, Application of minigenome technology in virology research of the Paramyxoviridae family, J. Microbiol. Immunol. Infect. 48 (2) (2015) 123–129, https://doi.org/10.1016/j.jmii.2014.02.008.
[17] Y. Peng, N. Du, Y. Lei, S. Dorje, J. Qi, T. Luo, et al., Structures of the SARS-CoV-2 nucleocapsid and their perspectives for drug design, EMBO J. 39 (20) (2020), e105938, https://doi.org/10.15252/embj.2020105938.
[18] J. Cubuk, J.J. Alston, J.J. Incicco, S. Singh, M.D. Stuchell-Brereton, M.D. Ward, et al., The SARS-CoV-2 nucleocapsid protein is dynamic, disordered, and phase separates with RNA, Nat. Commun. 12 (1) (2021), 1936, https://doi.org/10.1038/s41467-021-21953-3.
[19] C.R. Carlson, J.B. Asfaha, C.M. Ghent, C.J. Howard, N. Hartooni, M. Safari, et al., Phosphoregulation of phase separation by the SARS-CoV-2 N Protein suggests a biophysical basis for its dual functions, Mol. Cell. 80 (6) (2020) 1092–1103 e4, https://doi.org/10.1016/j.molcel.2020.11.025.
[20] C.K. Chang, M.H. Hou, C.F. Chang, C.D. Hsiao, T.H. Huang, The SARS coronavirus nucleocapsid protein–forms and functions, Antiviral Res 103 (2014) 39–50, https://doi.org/10.1016/j.antiviral.2013.12.009.
[21] C.J. Hsu, W.C. Lin, Y.C. Chou, C.M. Yang, H.L. Wu, Y.H. Cheng, et al., Dynamic changes of the blood chemistry in Syrian hamsters post-acute COVID-19, Microbiol. Spectr. 10 (1) (2022), e0236221, https://doi.org/10.1128/spectrum.02362-21.
[22] A. McBeath, N. Bain, M. Fourrier, B. Collet, M. Snow, A strand specific real-time RT-PCR method for the targeted detection of the three species (vRNA, cRNA and mRNA) of infectious salmon anaemia virus (ISAV) replicative RNA, J. Virol. Methods 187 (1) (2013) 65–71, https://doi.org/10.1016/j.jviromet.2012.09.007.
[23] A. Asada, H. Hayakawa, N. Yanase, K. Abe, F. Sakurai, H. Mizuguchi, et al., A flow cytometry-based method to determine the titer of adenoviruses expressing an extraneous gene, Biol. Pharm. Bull. 41 (10) (2018) 1615–1619, https://doi.org/10.1248/bpb.b18-00316.
[24] J.Y. Rathbun, M.E. Droniou, R. Damoiseaux, K.G. Haworth, J.E. Henley, C.M. Exline, et al., Novel Arenavirus entry inhibitors discovered by using a minigenome rescue system for high-throughput drug screening, J. Virol. 89 (16) (2015) 8428–8443, https://doi.org/10.1128/JVI.00997-15.
[25] J.H. Zhang, T.D. Chung, K.R. Oldenburg, A simple statistical parameter for use in evaluation and validation of high throughput screening assays, J. Biomol. Screen 4 (2) (1999) 67–73, https://doi.org/10.1177/108705719900400206.
[26] C. Wu, A.J. Qavi, A. Hachim, N. Kavian, A.R. Cole, A.B. Moyle, et al., Characterization of SARS-CoV-2 nucleocapsid protein reveals multiple functional consequences of the C-terminal domain, iScience 24 (6) (2021), 102681, https://doi.org/10.1016/j.isci.2021.102681.
[27] B. Zhang, J. Tian, Q. Zhang, Y. Xie, K. Wang, S. Qiu, et al., Comparing the Nucleocapsid proteins of human coronaviruses: structure, immunoregulation, vaccine, and targeted drug, Front. Mol. Biosci. 9 (2022), 761173, https://doi.org/10.3389/fmolb.2022.761173.
[28] Y.C. Wang, S.W. Lin, I.J. Wang, C.Y. Yang, C. Hong, J.R. Sun, et al., Interleukin-6 test strip combined with a spectrum-based optical reader for early recognition of COVID-19 patients with risk of respiratory failure, Front. Bioeng. Biotechnol. 10 (2022), 796996, https://doi.org/10.3389/fbioe.2022.796996.
[29] T. Hoenen, S. Jung, A. Herwig, A. Groseth, S. Becker, Both matrix proteins of Ebola virus contribute to the regulation of viral genome replication and transcription, Virology 403 (1) (2010) 56–66, https://doi.org/10.1016/j.virol.2010.04.002.
[30] T.K. Warren, R. Jordan, M.K. Lo, A.S. Ray, R.L. Mackman, V. Soloveva, et al., Therapeutic efficacy of the small molecule GS-5734 against Ebola virus in rhesus monkeys, Nature 531 (7594) (2016) 381–385, https://doi.org/10.1038/nature17180.

[31] L.D. Jasenosky, G. Neumann, Y. Kawaoka, Minigenome-based reporter system suitable for high-throughput screening of compounds able to inhibit Ebolavirus replication and/or transcription, Antimicrob. Agents Chemother. 54 (7) (2010) 3007–3010, https://doi.org/10.1128/AAC.00138-10.
[32] C.J. Gordon, E.P. Tchesnokov, E. Woolner, J.K. Perry, J.Y. Feng, D.P. Porter, et al., Remdesivir is a direct-acting antiviral that inhibits RNA-dependent RNA polymerase from severe acute respiratory syndrome coronavirus 2 with high potency, J. Biol. Chem. 295 (20) (2020) 6785–6797, https://doi.org/10.1074/jbc.RA120.013679.
[33] E.P. Tchesnokov, J.Y. Feng, D.P. Porter, M. Gotte, Mechanism of inhibition of Ebola virus RNA-dependent RNA polymerase by Remdesivir, Viruses 11 (4) (2019), https://doi.org/10.3390/v11040326.
[34] M.K. Lo, R. Jordan, A. Arvey, J. Sudhamsu, P. Shrivastava-Ranjan, A.L. Hotard, et al., GS-5734 and its parent nucleoside analog inhibit Filo-, Pneumo-, and Paramyxoviruses, Sci. Rep. 7 (2017), 43395, https://doi.org/10.1038/srep43395.
[35] B. Vanmechelen, J. Stroobants, K. Vermeire, P. Maes, Advancing Marburg virus antiviral screening: optimization of a novel T7 polymerase-independent minigenome system, Antiviral Res 185 (2021), 104977, https://doi.org/10.1016/j.antiviral.2020.104977.
[36] H. Yamada, S. Taniguchi, M. Shimojima, L. Tan, M. Kimura, Y. Morinaga, et al., M segment-based minigenome system of severe Fever with thrombocytopenia syndrome virus as a tool for antiviral drug screening, Viruses 13 (6) (2021), https://doi.org/10.3390/v13061061.
[37] H. Jerome, M. Rudolf, M. Lelke, M. Pahlmann, C. Busch, S. Bockholt, et al., Rift Valley fever virus minigenome system for investigating the role of L protein residues in viral transcription and replication, J. Gen. Virol. 100 (7) (2019) 1093–1098, https://doi.org/10.1099/jgv.0.001281.
[38] B.D. Griffin, A. Leung, M. Chan, B.M. Warner, C. Ranadheera, K. Tierney, et al., Establishment of an RNA polymerase II-driven reverse genetics system for Nipah virus strains from Malaysia and Bangladesh, Sci. Rep. 9 (1) (2019), 11171, https://doi.org/10.1038/s41598-019-47549-y.
[39] R. Flick, K. Flick, H. Feldmann, F. Elgh, Reverse genetics for crimean-Congo hemorrhagic fever virus, J. Virol. 77 (10) (2003) 5997–6006, https://doi.org/10.1128/jvi.77.10.5997-6006.2003.
[40] K. Flick, J.W. Hooper, C.S. Schmaljohn, R.F. Pettersson, H. Feldmann, R. Flick, Rescue of Hantaan virus minigenomes, Virology 306 (2) (2003) 219–224, https://doi.org/10.1016/s0042-6822(02)00070-3.